

PAPER

One-step selective laser patterning of copper/graphene flexible electrodes

To cite this article: Peng Peng *et al* 2019 *Nanotechnology* **30** 185301

View the [article online](#) for updates and enhancements.

You may also like


- [Laser direct-write of single microbeads into spatially-ordered patterns](#)
Theresa B Phamduy, Nurazhani Abdul Raof, Nathan R Schiele et al.
- [Recent progress of patterned electrodes in wearable electronics: fabrication and application](#)
Xin-Ran Zhang, Hai-Tao Deng, Xu Zeng et al.
- [Digital selective fabrication of micro/nano-composite structured TiO₂ nanorod arrays by laser direct writing](#)
Wei Jiang, Xiaoning He, Hongzhong Liu et al.



ECS
The
Electrochemical
Society
Advancing solid state &
electrochemical science & technology

DISCOVER
how sustainability
intersects with
electrochemistry & solid
state science research

One-step selective laser patterning of copper/graphene flexible electrodes

Peng Peng^{1,2} , Lihang Li¹, Peng He², Ying Zhu¹, Jian Fu¹, Yongde Huang³ and Wei Guo^{1,2}

¹ School of Mechanical Engineering and Automation, Beihang University, Beijing 100191, People's Republic of China

² State Key Laboratory of Advanced Welding and Joining, Harbin Institute of Technology, Harbin 150001, People's Republic of China

³ School of Aerospace Manufacturing Engineering, Nanchang Hangkong University, Nanchang, Jiangxi 330063, People's Republic of China

E-mail: gwei@buaa.edu.cn

Received 17 November 2018, revised 24 December 2018

Accepted for publication 14 January 2019

Published 18 February 2019



Abstract

Flexible electrodes have attracted much attention in consumer electronic applications. In this work, laser direct writing is used to fabricate copper/graphene composite electrodes on a flexible substrate in one step. This direct writing process with a low power laser can reduce copper ions in thin films to form copper nanomaterials and spontaneously interconnect them to gain good conductivity, while the laser also induces the growth of multi-layer graphene that coats on copper to improve the oxidation resistance of electrodes. The electrical performance and chemical composition of flexible electrodes can be tuned by laser power, scanning speed, and defocus distance. A mechanism of *in situ* reduction and interconnection of copper nanomaterials during laser direct writing has been proposed. This method could largely reduce the oxidation issue by avoiding synthesis and sintering processes of copper nanomaterials. These as-written copper electrodes have good stability and have potential applications in flexible electronics, such as flexible heaters or antennas as demonstrated.

Keywords: laser direct writing, copper nanomaterials, graphene, *in situ* reduction, nanojoining

(Some figures may appear in colour only in the online journal)

1. Introduction

Flexible electrodes can be used in many applications, such as wearable devices [1, 2], solar cells [3, 4], touch screens [5, 6], etc. They are usually based on highly conductive materials, such as silver [4, 7], gold [8], and indium tin oxides (ITOs) [9]. Owing to the development of printing technology with nanoparticles (NPs) [10–12], nanowires (NWs) [6, 13, 14], and core-shell NWs [15], selective patterning of electrodes on flexible substrates can be realized for fabricating flexible devices. However, because gold and silver are expensive and ITO is brittle during deformation, it is necessary to find other alternatives for practical applications. Recently, copper (Cu) nanomaterials have emerged as a potential material for flexible electronics due to its good electrical/thermal properties and economical merits [16, 17]. Usually, such Cu

nanomaterial based electrodes start with the synthesis of Cu nanomaterials that are sintered together using heat [18], laser [10], or chemicals [16] later to meet the conductivity requirement. Due to their large surface to volume ratio, oxidation of Cu nanomaterials is more difficult than bulk Cu. In order to tackle this problem, a commonly used method is covering Cu nanomaterials with a layer of protective materials, such as polymer [18] or carbon materials [19]. However, it complicates the fabrication process and such introduced protective layer would present at the interface of the Cu nanomaterials, which would impede the electron from passing through unless high temperature sintering in inert gas or vacuum is used to decompose it and interconnect Cu nanomaterials [20, 21]. Unfortunately, this high temperature sintering process is undesirable for industry and could cause electrode delamination or damage of flexible substrates

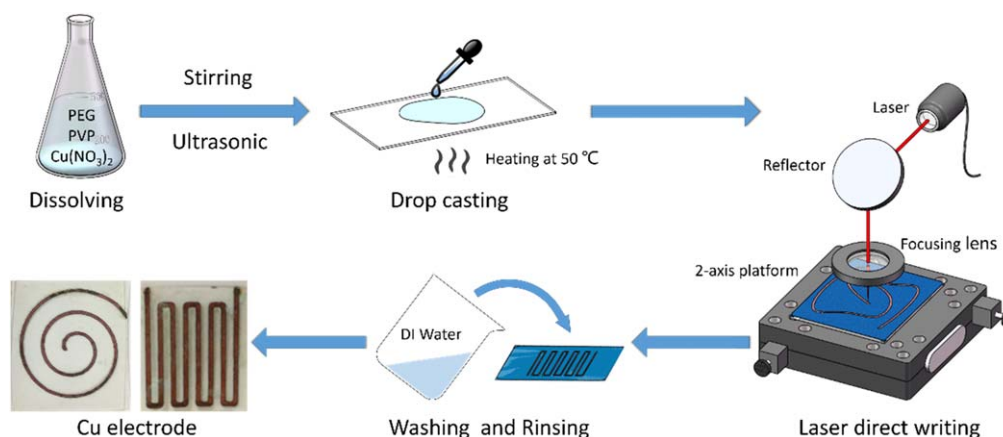


Figure 1. Schematic of the laser selective patterning Cu electrodes.

[18, 22], and is also difficult to implement area-selection precisely. So far, many attempts have been reported to replace high temperature thermal sintering, such as intense pulsed light sintering [23] and the selective laser sintering/welding process [24, 25]. These methods can pattern Cu electrodes quickly, but the problem of the easy oxidation of Cu nano-materials in fabrication, processing and subsequent application, has yet to be solved.

To address this issue, CuO or Cu₂O NPs, Cu ions have been used as a Cu source to synthesize Cu NPs and sinter them together with thermal heating or intense pulsed light [10, 23, 26, 27], because they are much more stable than Cu NPs in ambient conditions [23]. This method not only simplifies the steps of synthesis, but also has the advantages of operating at room temperature, is environmentally friendly, and produces less impurities. Further, combined with the laser direct writing technique, it can achieve rapid processing and selective patterning.

In this study, a Cu ion thin film is prepared on a flexible substrate, and then Cu ions are reduced to Cu nanomaterials and interconnected spontaneously by laser direct writing for selective patterning of Cu electrodes. Water-soluble Cu ion thin film is facile to fabricate and stable in atmosphere, and non-irradiated areas can be easily removed after patterning. Laser direct writing can also produce amorphous carbon or graphene in the as-fabricated electrodes. The influence of the laser parameters on the electrical performance and chemical composition of flexible electrodes are investigated. The application of such as-written Cu electrodes has also been demonstrated in flexible resistive heaters and antennas.

2. Methods

2.1. Patterning of Cu electrodes

The Cu ion ink contained 10 ml of deionized (DI) water, 0.97 g copper (II) nitrate hydrate ($\text{Cu}(\text{NO}_3)_2 \cdot 3\text{H}_2\text{O}$), 0.1 g polyvinyl pyrrolidone (PVP, K30, $M_w \approx 40\,000\text{ g} \cdot \text{mol}^{-1}$), and polyethylene glycol (PEG). All reagents were purchased from Sinopharm Chemical Reagent Co. Ltd. Before coating, the surface of the polycarbonate (PC) substrate was treated

with oxygen plasma to enhance the substrate's hydrophilicity. First, the as-prepared Cu ion ink was drop-casted on the PC substrate followed by drying in an oven at 50 °C. The process of laser direct writing was conducted using a continuous wave diode laser (K808DAHFN-20.00 W, BWT Beijing Ltd) with a wavelength of 808 nm. The reflector is a protective silver reflector, and the focusing lens is a k9 flat convex lens ($f = 25\text{ cm}$). After selective patterning, the non-irradiated areas were washed with DI water since the Cu ion film is water soluble, leaving the as-patterned Cu electrodes on PC substrates.

2.2. Characterization

The microstructure and morphology were characterized by field emission scanning electron microscopy (Merlin Compact, Germany) and an optical microscope (OM, Carl Zeiss, Germany). To analyze the chemical composition of the electrodes, x-ray diffraction (XRD, Rigaku D/max, Japan), and Raman spectrum (inVia-Reflex, Renishaw, the UK) were measured. The electrical properties of Cu electrodes were tested by a digital source meter (Keithley, 2400, USA).

3. Results and discussion

Figure 1 illustrates the processes of the coating of the Cu ion film and the laser direct writing of the Cu electrodes. The Cu ion ink was drop-casted on the PC substrate followed by drying. After selective patterning by laser direct writing, the non-irradiated areas could be washed with DI water since the Cu ion film is water soluble, leaving the as-patterned Cu electrodes on the PC substrates. Figures 2(a) and (b) depict the change in the Cu ion thin film after laser direct writing. After irradiation, the blue film changed into a reddish color, typical of Cu, while the thickness was reduced from 140–130 μm as illustrated in figures 2(a) and (b). Meanwhile, the sheet resistance of the irradiated area decreased to less than $1\,\Omega \cdot \text{sq}^{-1}$. Because the temperature is very low during laser scanning (as shown in figure 2(c)), the measured macroscopic temperature during laser direct writing is only about 40 °C, the reduction of Cu^{2+} is unlikely due to the generation

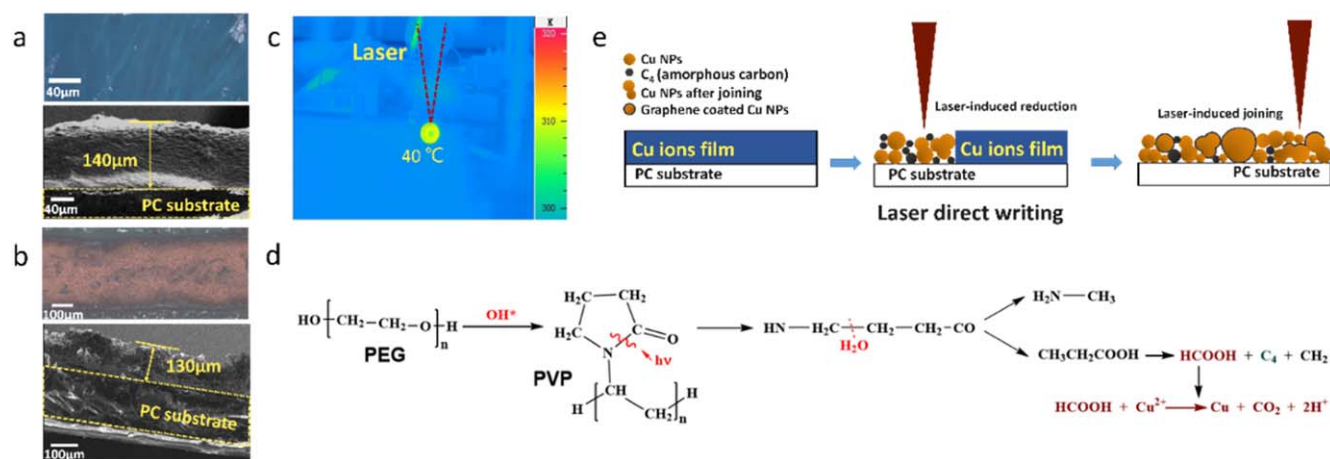


Figure 2. The OM image and the scanning electron microscopy (SEM) image (side view) of Cu ion thin film (a) before and (b) after laser irradiation. (c) Snap-shot of temperature distribution on the C substrate during laser direct writing measured with an infrared camera. Schematics of (d) laser induced chemical reduction, and (e) the structural change during laser induced reduction and joining of Cu nanomaterials.

of aldehydes, which requires a temperature of at least 180 °C [17, 27, 28]. To validate this, direct thermal heating of the Cu²⁺ film in an oven was conducted. The results indicate that even 200 °C oven heating is impossible to produce Cu⁰. As presented in the schematic mechanism of the reduction of figure 2(d), the laser irradiation can convert the PVP ring structure into methylene, methylamine, and propanoic acid through photodegradation with the assistance of the OH radical coming from the PEG [28, 29], and the methylamine and propanoic acid can come from the hydrolysis [29]. The propanoic acid could further decompose into formic acid, and then react with Cu²⁺ to generate Cu⁰ [23, 30]. Simultaneously, carbon dioxide and amorphous carbon were also generated during this reaction [28]. It is interesting that this amorphous carbon could present in the electrodes or grow into graphene wrapped on Cu particles (as illustrated in figure 2(e)) since the Cu can act as a catalyst and substrate [31], which will be discussed later in detail. The interconnection of the generated Cu nanomaterials will also occur through laser induced *in situ* joining to improve the conductivity of as-fabricated electrodes.

The electrical property of the laser-irradiated area is very sensitive to the parameters of the laser direct writing process. Figure 3(a) shows the dependence of the laser power and the sheet resistance with two different laser defocus distances (0 and 6 mm). Overall, the sheet resistance, with the increase of laser power, presents a trend of first descending and then rising. The processing window of the laser power for obtaining Cu electrodes with good conductivity varies with laser defocus distance. Laser power from 1–4.5 W is appropriate for a defocus distance of 0 mm, while it is 1.5–5 W for a defocus distance of 6 mm. When the laser power is relatively low (<1 or 1.5 W), the laser-irradiated areas are non-conductive with a sheet resistance larger than 10 kΩ because Cu²⁺ have not been reduced. When the laser power was beyond 4.5 or 5 W, the substrate was damaged because of the overheating caused by the high energy of the laser. The minimum sheet resistance is 2.53 Ω · sq⁻¹ at 2.5 W for a

defocus distance of 0 mm, while this value is 0.17 Ω · sq⁻¹ at 4 W for a defocus distance of 6 mm. These sheet resistances are similar as the reported values of 0.3–0.5 Ω · sq⁻¹ for laser sintered Cu NP electrodes [25, 32], and 0.11 Ω · sq⁻¹ for thermal sintered Cu NW at 220 °C [33], as summarized in table 1. This suggests that laser direct writing can realize the rapid fabrication of Cu flexible electrodes with high conductivity while the process is much simpler with only one step, working at near room temperature, and involves no pre-synthesis of NPs or NWs.

Figures 3(b) and (c) indicate the dependence of sheet resistance with laser scanning speed and defocus distance. As depicted in figure 3(b), the resistance decreases first and then increases as the scanning speed increases similar to the effect of laser power. Particularly, a scanning speed from 3–20 mm s⁻¹ is an appropriate processing window in this study. To study the effect of the defocus distance during laser direct writing, the resistance of the patterned electrodes at various laser defocus distances, when the laser power is 3.5 W and the scanning speed is 5 mm s⁻¹, is measured as plotted in figure 3(c). The sheet resistance decreases with the increase of defocus distance, and the value is as low as 0.17 Ω · sq⁻¹ when the defocus distance is 6 mm. If continually increasing the defocus distance over 6 mm, the sheet resistance rises up slowly but generally it is maintained below 3 Ω · sq⁻¹ when the defocus distance exceeds 4 mm. It is worth noting that the change in the defocus distance will cause the enlargement of the size of laser spot, which determines the line width of the Cu electrode after laser direct writing. Figure 3(d) shows the *V-I* characteristic curves of patterned electrodes under different laser parameters. The *V-I* curves under different laser parameters display good linear Ohmic characteristics. The slope of the *V-I* curves varies obviously with the laser parameters representing the different conductivity. Therefore, by controlling the laser power, scanning speed, or defocus distance, tuning the laser energy density, in other words, electrodes with different sheet resistance and line width can be obtained. The sheet resistance could vary from 0.17–40 Ω · sq⁻¹, indicating the

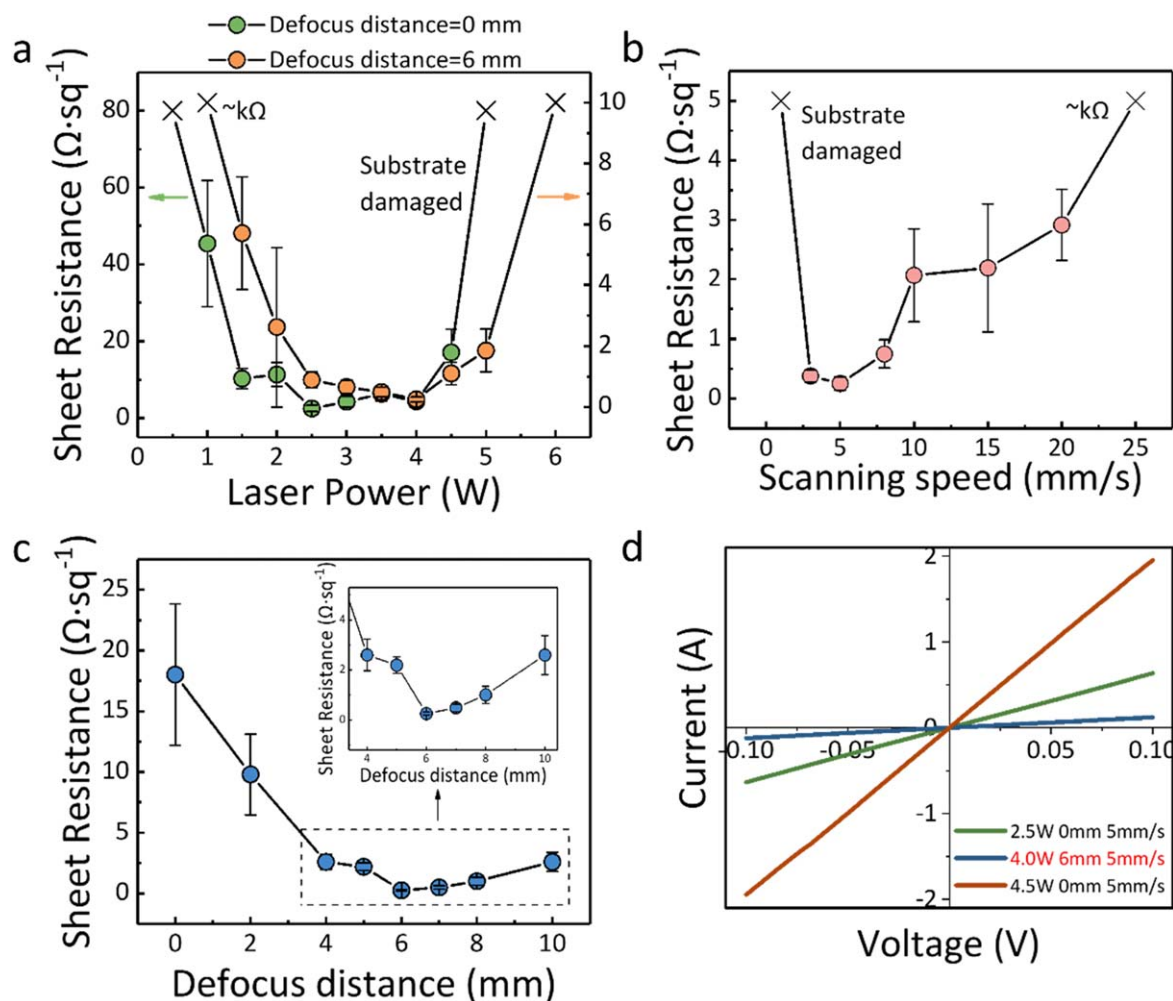


Figure 3. Electrical properties of Cu electrodes under different laser parameters. The changes in sheet resistance (a) with the laser power in two defocus distances (0 and 6 mm) when the scanning speed is 5 mm s^{-1} , (b) with the scanning speed when the laser power is 4 W and the defocus distance is 6 mm, (c) with the defocus distance when the laser power is 4 W and the scanning speed is 5 mm s^{-1} . (d) The V - I (voltage–current) characteristic curve of patterned electrodes under different laser parameters.

Table 1. Comparison of the resistivity of electrodes using different Cu sources.

Materials	Substrate	Resistivity ($\Omega \cdot \text{m}$)	Sheet resistance (Ω/sq)	References
Cu bulk	—	1.678×10^{-8}	—	—
Cu NPs	PI/PEN	$(2-8) \times 10^{-7}$	0.3–0.5	[22, 28]
Cu NWs	PI/filter paper	—	15–0.11 (220 °C)	[16, 34]
CuO NPs	PI	3.1×10^{-7}	0.14	[32]
$\text{Cu}(\text{OH})(\text{NO}_3)/\text{Cu}(\text{NO}_3)_2$	PET	2.4×10^{-6}	—	[8]
$\text{Cu}(\text{NO}_3)_2$	PC	3.4×10^{-6}	0.17	This work

possibility of fabricating Cu structures with various resistances in one step by changing the laser parameters.

To understand the conductivity of patterned Cu electrodes, chemical compositions are measured using XRD and Raman spectroscopy. As illustrated in figure 4(a), all regions irradiated with a low power laser (1.5 W) present the color of metallic Cu. Although the laser irradiation regions with different parameters could mostly be conductive, a black area appears in the middle portion under a higher laser power of 4.5 W (figure 4(a)), which might be the reason for the increase in

sheet resistance. This black region is due to the high laser intensity because of the Gaussian distribution of the laser beam. Micron-sized spheres can be observed in this region with a film wrapped over the surface. Characterized by energy-dispersive X-ray spectroscopy EDS analysis, the sphere consists of a surface carbon shell and an internal Cu core (location I: 85% of C and 15% of Cu, location II: 98% of C and 2% of Cu), which suggests the formation of carbon film during laser direct writing. The XRD patterns in figure 4(b) indicate that the electrodes are metal the Cu and Cu_2O phases under the laser

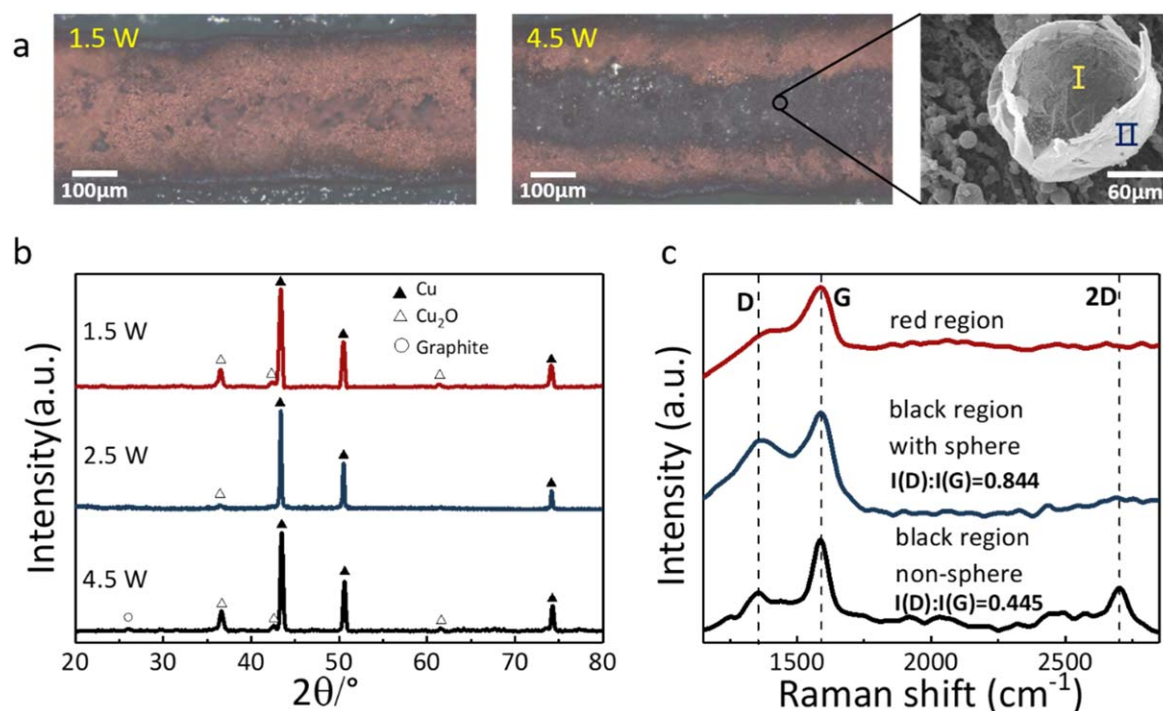


Figure 4. (a) OM images of Cu electrodes at 1.5 and 4.5 W and the SEM image of the black region. (b) The XRD patterns of Cu electrodes fabricated at 1.5, 2.5, and 4.5 W. (c) The Raman spectra of different regions in the electrodes.

powers of 1.5 and 4.5 W. When the laser power is 2.5 W, the electrode mainly contains Cu metal with an almost invisible Cu₂O phase. The three diffraction peaks at 43.5°, 50.7°, and 74.4° correspond to the (111), (200), and (220) planes of the Cu phase, respectively, while the three diffraction peaks at 36.6°, 42.6°, and 61.3° belong to the Cu₂O phase [23, 27]. The calculated ratio of the Cu₂O/Cu phase varies with different laser powers (0.221 for 1.5 W, 0.153 for 2.5 W, and 0.336 for 4.5 W). By comparing their sheet resistances (10.32 Ω · sq⁻¹ for 1.5 W, 2.53 Ω · sq⁻¹ for 2.5 W, and 17.13 Ω · sq⁻¹ for 4.5 W), it can be found that the sheet resistance is proportional to the ratio of Cu₂O/Cu, suggesting the composition and electrical conductivity of patterned Cu electrodes could be controlled by playing with laser power. Here, the increase of Cu₂O might lead to a decline in electrical conductivity, which might be due to the uncompleted reduction of Cu²⁺ at low laser power or the oxidation of Cu at high laser power during laser direct writing. In addition, there is a weak peak at 26.6° corresponding to graphite under the laser power of 4.5 W, which confirms the existence of crystallized carbon film as observed on the surface of the micron-sized spheres. It is also worth noting that no CuO phase has been detected in either the low and high laser power cases, suggesting such a black region at 4.5 W is not due to the oxidation of Cu.

Furthermore, two typical Raman peaks of carbon materials are observed at 1370 and 1585 cm⁻¹ referred as the D and G bands of graphite [35, 36] in all regions of the patterned Cu electrodes (figure 4(c)). The appearance of the G band represents that the structure of the wrapped carbon shell on the Cu sphere is mainly a plane structure of graphite (sp²-hybridized carbon), while the D band shows the presence

of defects in the graphitic lattice [8, 37]. The D band of red regions is almost invisible but the G band can be observed clearly. Generally, the $I(D)/I(G)$ ratio indicates the defects and disordered structure of graphite or multi-layered graphene. The I_D value of non-defected graphene or graphite is relatively small as compared to other carbonaceous structures, such as amorphous carbon [36, 37]. Consequently, the presence of the G band in the red region indicates the generation of graphite. The D and G bands both can be observed in the black regions, but the $I(D)/I(G)$ ratio of the non-spherical region is lower than that of the with-sphere region, and increased from 0.445–0.844. Therefore, more structural changes and defects existed in the with-sphere region than the non-spherical region, because more sp³-hybridized carbon might be formed in a spherical structure [8, 37].

Figure 5(a) displays the spherical structure in the Cu electrode at high laser power. Similar to the spherical structure in figure 4(a), the surface of the sphere is wrapped with a layer of transparent film composed of carbon. The surface wrinkles can be observed clearly in the insert of the high magnification image, which is similar to the morphology of graphene. Figure 5(b) is the C1s XPS pattern of the Cu electrode. The C1s peak at 284.8 eV is identified as C–C or C=C, confirming the existence of graphene (or graphite) [8]. The peak at 286.4 eV and 288.6 eV are identified as C–O and COO–, respectively. This may be caused by residual PVP, PEG, and carboxylic acids or graphene oxide generated after laser irradiation. The transmission electron microscopy (TEM) image shown in figure 5(c) shows that Cu NPs (as shown by yellow circle) are wrapped with film-like structure. These NPs with a (111) lattice of 2.07 Å are very small,

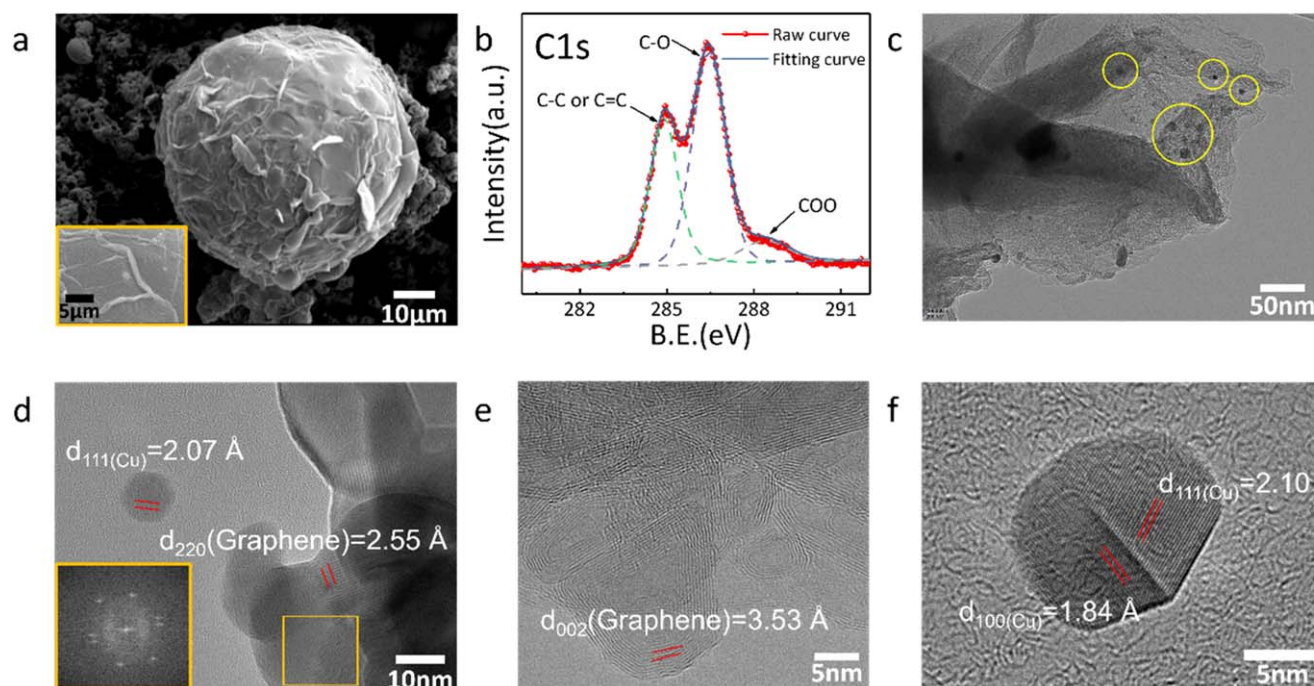


Figure 5. (a) Graphene sheets coated on Cu particles observed in the electrode. Inset: high magnification image of the surface. (b) The C1s XPS pattern and (c)–(f) TEM images of the Cu/graphene electrode.

~10 nm, see figure 5(d). The high resolution TEM images of the Cu electrode display sheet structures of the carbon film with a lattice spacing of 2.55 Å, corresponding to the hexagonal lattice plane spacing d_{220} of graphite, see figure 5(d). The corresponding fast Fourier transform pattern in the inset of figure 5(d) illustrates a single 6-fold symmetric diffraction pattern, indicating the orientation of the hexagonal graphene network [38, 39]. Figure 5(e) confirms a typical multi-layer graphene structure with $d_{002} = 3.53$ Å [40, 41]. A typical interconnected interface of two Cu NPs is also presented in figure 5(f), whose connection is attributed to laser induced joining. The observed 2.10 and 1.84 Å lattices belong to the (111) and (200) planes of Cu [18, 42]. Herein, this one-step laser direct writing on Cu ion film could induce the reduction to get Cu nanomaterials and *in situ* joining to form conductive electrodes. It might be of great interest that this photon reaction process could stimulate the carbonization of organics and grow graphene sheets on as-formed Cu nanomaterials because Cu can serve as a catalyst during the growth [31, 43].

To understand the joining process of Cu NPs in laser direct writing, figure 6 illustrates the changes of the microstructure of the Cu electrodes. Figure 6(a) indicates the difference in the microstructure between the red and black regions. The red regions are mainly a network distributed on both sides of the Cu electrode corresponding to the low energy density area of the laser beam, while the black region is a spherical structure in the middle of the Cu electrode because of the Gaussian distribution of the laser. At high laser energy density, the black region with the presence of multi-layered graphene is formed, while the red region is dominated by Cu with little graphene under low laser energy density (as shown by the C1s XPS results in figure 5(b)). Figure 6(b)

shows a typical sintered structure of Cu nanomaterials in electrodes under low laser energy density. The laser induces the reduction of the Cu^{2+} into the Cu NPs and the interconnection of such NPs together, to form a network structure accompanied by some gas emission possibly, as suggested in figure 2(d). As laser energy density increases, the Cu structure could melt under high local heating temperature induced by laser and solidify into a large sphere due to the assistance of surface tension, as shown in figure 6(c). Usually, the melting of Cu NPs requires a high temperature, but here the macroscopic temperature is only 40 °C according to the measurement (see figure 2(c)). It seems impossible to melt Cu NPs. However, the surface plasmon effect [44, 45] induced by a laser would enhance the local temperature greatly at the contact area of the Cu NPs to promote melting [34, 46]. The jagged holes in the spherical structure also indicates that it is formed by merging of multiple Cu NPs. In these micro-sized spheres, the content of carbon is below 5% as shown by the EDS analysis. As the laser energy density increases further, black regions appear in the center of Cu electrodes and the content of carbon increases. Figure 6(d) shows the surface of the formed spheres in the black regions, illustrating a carbon shell on an internal Cu sphere. According to the EDS analysis, the proportion of Cu and carbon is about 40:60. Although EDS is a semiquantitative analysis, it still shows the significantly different composition from the change tendency of the Cu and carbon ratio. The increase in carbon content indicates an increase in the degree of carbonization.

The microstructures are closely related to the electrical properties because the increase in conductivity is derived from the connection of Cu NPs. At first, the laser induces an interconnection between the Cu nanomaterials to form a

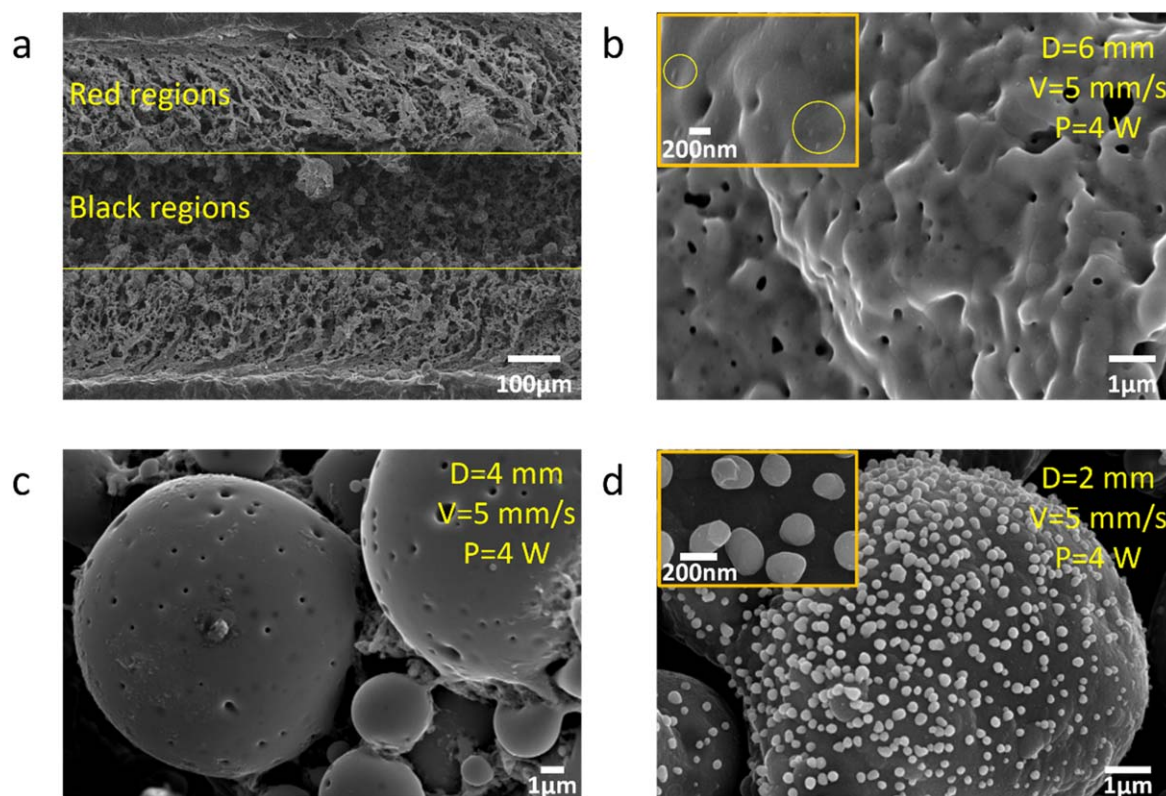


Figure 6. (a) Two regions of as-patterned electrode. (b)–(d) High resolution SEM images electrodes fabricated from low to laser energy density by changing the defocused distance (D). The inset in (b) and (d), detailed tiny NPs on the surface.

network structure, which greatly enhances the conductivity of the electrodes. With the increase in laser energy density, the higher local temperature caused by the surface plasmon effect creates more intense joining between Cu NPs or even melting to further transform a network structure into large spheres. Such large spheres cause less interconnection area in electrodes, leading to a slight decrease of electrical conductivity. As the laser energy density continually increases, the multi-layered graphene structure will be present in the electrodes and cover the surface of as-formed Cu spheres. Although the conductivity of graphene is very good in plane (resistivity Cu at 20 °C is $1.678 \times 10^{-8} \Omega \cdot \text{m}$, graphene is $10^{-8} \Omega \cdot \text{m}$, graphite parallel to layer is $2.5\text{--}5.0 \times 10^{-6} \Omega \cdot \text{m}$, and graphite perpendicular to layer is $3 \times 10^{-3} \Omega \cdot \text{m}$ [47, 48]), it presents at the interface of Cu spheres with limited contribution to the improvement in conductivity. Moreover, there are many defects in the graphene (as the Raman spectroscopy results indicate in figure 4(c)) produced by this laser process, resulting in an obvious decline in conductivity.

Some tiny Cu NPs are observed on the surface of the sphere (the inset in figure 6(d)), which may be formed by rapid solidification of Cu during laser scanning. Also, the similar ultra-small particles can also be found on the surface of the network structure, highlighted by a bright yellow circle in the inset of figure 6(b). Nevertheless, the size of the particles at low laser energy density is much smaller than that of high energy density. Two reasons can explain the growth of such tiny NPs. The first is that there is a difference in the thermal conductivity of graphene and Cu. The measured

thermal conductivity of single layer graphene is in the range 3000–5000 W/(m · K) at room temperature [48], and the thermal conductivity of Cu is 401 W/(m · K) respectively [48]. Because, after the laser scanning, the local heat transfers faster in the graphene wrapped Cu than in the Cu network, such Cu NPs on the surface of the graphene will be more easily aggregated. The second is that the wettability of the same material is better than that of the dissimilar material. Therefore, the Cu NPs attached to the surface are easily formed on the graphene because the wetting angle is an obtuse angle [49].

Figure 7 shows the oxidation resistance of patterned Cu/graphene electrodes. Figure 7(a) indicates the change in conductivity in 24 h at different temperatures. The rate of change of the resistance is below 20% when the temperature is under 80 °C, showing good reliability. However, when the temperature reaches above 110 °C, the oxidation will increase the resistance rapidly, eventually resulting in no conductivity. Figure 7(b) displays the change in conductivity with aging time at 25 °C and 50 °C. Under different temperature conditions, the resistance shows a different trend with time. At 25 °C, the rate of change of the resistance rises almost linearly with time. While for the electrodes fabricated with different laser power aging at 50 °C, the resistance remains unchanged within the first 5 days, and it increases rapidly from 5–15 days, and becomes stable after 15 days as shown in figure 7(b). At first, a very thin natural Cu₂O layer could form on the surface of the Cu electrodes [33, 50] to prevent further oxidation, which contributes to the unchanged conductivity

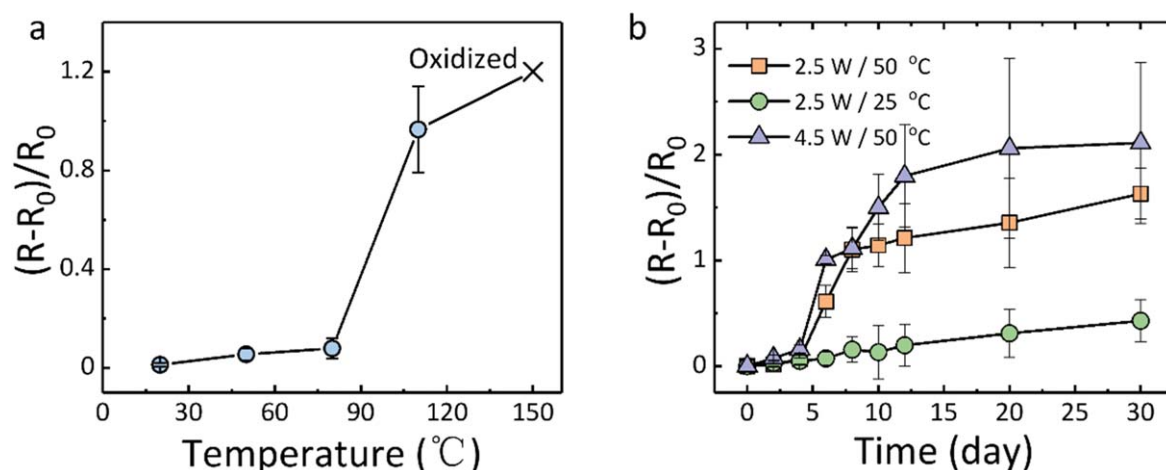


Figure 7. (a) The electrical conductivity of electrodes heating at different temperatures in air for 24 h. (b) The electrical conductivity of electrodes with different aging times at 25 °C-35%(RH) and 50 °C-20%(RH).

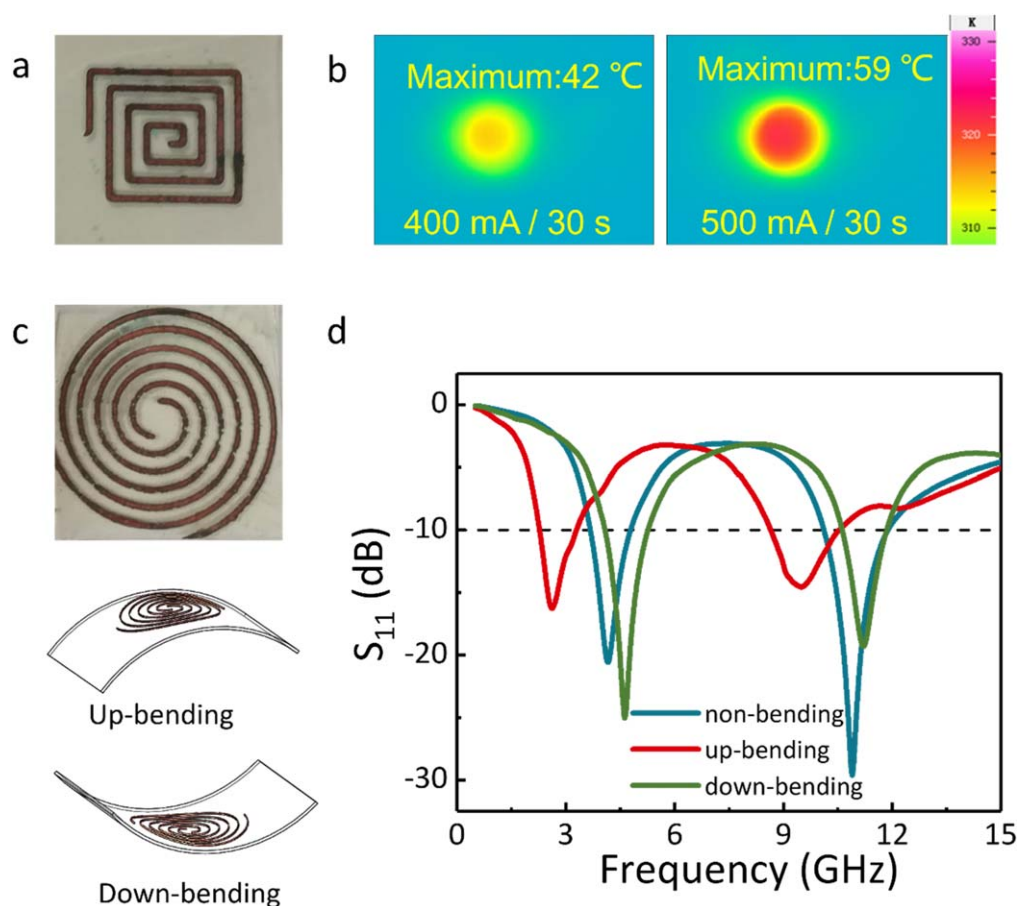


Figure 8. (a) Photograph of rapid heater on PC substrate, and (b) temperature distribution under different current conditions (400 and 500 mA) measured with an infrared camera. (c) Photograph of planar antenna on PC substrate, and (d) measured reflection (S_{11}) against frequency for various bending conditions of planar antenna.

over 5 days. Although these electrodes have no additional protection, the oxidation resistance is comparable to PMMA coated Cu NW or Cu core-shell particle electrodes [51, 52]. The rate of change of the resistance remains below 0.5 for 30 days when aged at 25 °C-35%(RH) (30 days in reference [33] for the Cu NW electrode with PMMA coating) and remains unchanged for 6 days at 50 °C-20%(RH) (5 days in reference

[52] for the Cu core particle electrode). Furthermore, the rate of change of the resistance is 0.07 for 24 h at 80 °C-10%(RH) (1 h in reference [52] for Cu NWs and 100 min for the Cu NW electrode with PMMA coating). This is probably because the graphene film (see figures 4(a) and 5) enhances the oxidation resistance [53] and maintains its good conductivity. Unavoidably, any type of Cu electrode will not be absolutely

free from oxidation in air. Therefore, the thin oxide layer become gradually thicker and the sheet resistance of the electrode increases with the passage of preserved time [33, 50], and the rise in temperature may accelerate this process.

As a proof of concept, the fabricated Cu/graphene electrode can be applied for various electronic applications. First, it is used as a flexible rapid heater, as shown in figure 8(a). Because of the thermal effect of the current, it can rapidly heat up when passing a steady current. The area where the temperature rises is the same size as the electrode, but the temperature in the center is slightly higher. In 30 s, a current of 400 mA can heat it up to 42 °C (figure 8(b)), while the 500 mA current can reach 59 °C (figure 8(b)). Also, the as-fabricated Cu/graphene flexible electrodes can be used as a flexible planar antenna for the detection of electromagnetic waves, as shown in figure 8(c). Figure 8(d) presents the S_{11} measurement curves of planar antennas under different bending conditions. In the unbending condition, the frequency bandwidth of this antenna is 3.6–4.8 GHz and 10.1–11.8 GHz. The frequency bandwidths will shift to low frequency in up-bending (2.2–3.3 GHz and 8.6–10.6 GHz), and shift to high frequency in down-bending (4.1–5.3 GHz and 10.6–11.8 GHz). This reflects the frequency conversion characteristics of the antenna and can expand its application range.

4. Conclusion

In summary, one-step fabrication of Cu/graphene flexible electrodes with a low sheet resistance of 0.17 Ω/sq at low temperature in ambient condition has been realized using laser direct writing. It can avoid the complex steps of synthesizing Cu nanomaterials and sintering. Laser could induce the *in situ* formation and joining of Cu nanomaterials as well as the growth of graphene sheets. Through this process, the sheet resistance could be reduced significantly and be controlled by changing the chemical composition and micro-structure of Cu/graphene electrodes through varying laser direct writing parameters. The reliability at different oxidation conditions are better than sintered Cu NP or NW electrodes due to the one-step and near room-temperature process, as well as the graphene film presented in electrodes. Finally, the rapid heater and planar antenna were fabricated to demonstrate the applicability in practical flexible devices.

Acknowledgments

We acknowledge funding from the National Key R&D Program of China (2017YFB1104900), the National Natural Science Foundation of China (Grant No. 51605019), the State Key Laboratory of Advanced Welding and Joining, Harbin Institute of Technology (AWJ-16-M05), the Key R&D Program of Jiangxi, China (20171BBE50010), and the Science and Technology Innovation Talents Program of Henan Province (Grant No. 174200510010). P.P. would like to thank

Dr Xiaodong Zhuge from the School of Electronic and Information Engineering, Beihang University for help with the antenna testing.

ORCID iDs

Peng Peng  <https://orcid.org/0000-0003-4455-1421>

References

- [1] Han S, Kim M K, Wang B, Wie D S, Wang S and Lee C H 2016 Mechanically reinforced skin-electronics with networked nanocomposite elastomer *Adv. Mater.* **28** 10257–65
- [2] Wang Q, Jian M, Wang C and Zhang Y 2017 Carbonized silk nanofiber membrane for transparent and sensitive electronic skin *Adv. Funct. Mater.* **27** 1605657
- [3] Li K, Zhen H, Niu L, Fang X, Zhang Y, Guo R, Yu Y, Yan F, Li H and Zheng Z 2014 Full-solution processed flexible organic solar cells using low-cost printable copper electrodes *Adv. Mater.* **26** 7271–8
- [4] Yang L, Zhang T, Zhou H, Price S C, Wiley B J and You W 2011 Solution-processed flexible polymer solar cells with silver nanowire electrodes *ACS Appl. Mater. Interfaces* **3** 4075–84
- [5] Kim T, Kim Y W, Lee H S, Kim H, Yang W S and Suh K S 2013 Uniformly interconnected silver-nanowire networks for transparent film heaters *Adv. Funct. Mater.* **23** 1250–5
- [6] Li R, Hu A, Zhang T and Oakes K D 2014 Direct writing on paper of foldable capacitive touch pads with silver nanowire inks *ACS Appl. Mater. Interfaces* **6** 21721–9
- [7] Guo W, Zeng Z, Zhang X, Peng P and Tang S 2015 Low-temperature sintering bonding using silver nanoparticle paste for electronics packaging *J. Nanomater.* **2015** 10
- [8] Li R Z, Peng R, Kihm K D, Bai S, Bridges D, Tumuluri U, Wu Z, Zhang T, Compagnini G and Feng Z 2016 High-rate in-plane micro-supercapacitors scribed onto photo paper using *in situ* femtosecond laser-reduced graphene oxide/Au nanoparticle microelectrodes *Energy Environ. Sci.* **9** 1458–67
- [9] Lee M, Jo Y, Kim D S, Jeong H Y and Jun Y 2015 Efficient, durable and flexible perovskite photovoltaic devices with Ag-embedded ITO as the top electrode on a metal substrate *J. Mater. Chem.* **3** 14592–7
- [10] Arakane S, Mizoshiri M, Sakurai J and Hata S 2017 Direct writing of three-dimensional Cu-based thermal flow sensors using femtosecond laser-induced reduction of CuO nanoparticles *J. Micromech. Microeng.* **27** 055013
- [11] Peng P, Hu A, Gerlich A P, Zou G, Liu L and Zhou Y N 2015 Joining of silver nanomaterials at low temperatures: processes, properties, and applications *ACS Appl. Mater. Interfaces* **7** 12597–618
- [12] Peng P, Li L, Guo W, Hui Z, Fu J, Jin C, Liu Y and Zhu Y 2018 Room-temperature joining of silver nanoparticles using potassium chloride solution for flexible electrode application *J. Phys. Chem. C* **122** 2704–11
- [13] An C-H, Kim S, Lee H-J and Hwang B 2017 Facile patterning using dry film photo-resists for flexible electronics: Ag nanowire networks and carbon nanotube networks *J. Mater. Chem. C* **5** 4804–9
- [14] Zhuang H, Yangai L, Wei G, Lihang L, Nan M, Chao J, Ying Z and Peng P 2017 Chemical sintering of direct-written silver nanowire flexible electrodes under room temperature *Nanotechnology* **28** 285703
- [15] Ting Y H, Chen J Y, Huang C W, Huang T K, Hsieh C Y and Wu W W 2018 Observation of resistive switching behavior in crossbar core-shell Ni/NiO nanowires memristor *Small* **14** 1703153

- [16] Kwon J, Cho H, Suh Y D, Lee J, Lee H, Jung J, Kim D, Lee D, Hong S and Ko S H 2017 Flexible and transparent Cu electronics by low-temperature acid-assisted laser processing of Cu nanoparticles *Adv. Mater. Technol.* **2** 1600222
- [17] Park J H *et al* 2017 Plasmonic-tuned flash Cu nanowelding with ultrafast photochemical-reducing and interlocking on flexible plastics *Adv. Funct. Mater.* **27** 1701138
- [18] Li Y, Huo Y, Li C, Xing S, Liu L and Zou G 2015 Thermal analysis of Cu-organic composite nanoparticles and fabrication of highly conductive copper films *J. Alloys Compd.* **649** 1156–63
- [19] Wang S, Tian H, Pei Y, Meng Q, Chen J, Wang H Z, Zeng Y, Zheng W and Liu Y 2012 Controllable synthesis of a novel hedgehog-like core/shell structure *J. Solid State Chem.* **186** 235–9
- [20] Jang S, Seo Y, Choi J, Kim T, Cho J, Kim S and Kim D 2010 Sintering of inkjet printed copper nanoparticles for flexible electronics *Scr. Mater.* **62** 258–61
- [21] Kang J S, Kim H, Ryu J, Hahn H T, Jang S and Joung J W 2010 Inkjet printed electronics using copper nanoparticle ink *J. Mater. Sci., Mater. Electron.* **21** 1213–20
- [22] Li Y, Li D, Li C, Wang H, Shen D, Liu L and Zou G 2015 Annealing-induced highly-conductive and stable Cu-organic composite nanoparticles with hierarchical structures *J. Alloys Compd.* **636** 1–7
- [23] Wang B Y, Yoo T H, Song Y W, Lim D S and Oh Y J 2013 Cu ion ink for a flexible substrate and highly conductive patterning by intensive pulsed light sintering *ACS Appl. Mater. Interfaces* **5** 4113–9
- [24] Han S, Hong S, Ham J, Yeo J, Lee J, Kang B, Lee P, Kwon J, Lee S S and Yang M 2014 Fast plasmonic laser nanowelding for a Cu-nanowire percolation network for flexible transparent conductors and stretchable electronics *Adv. Mater.* **26** 5808–14
- [25] Kwon J, Cho H, Eom H, Lee H, Suh Y D, Moon H, Shin J, Hong S and Ko S H 2016 Low-temperature oxidation-free selective laser sintering of Cu nanoparticle paste on a polymer substrate for the flexible touch panel applications *ACS Appl. Mater. Interfaces* **8** 11575–82
- [26] Arakane S, Mizoshiri M and Hata S 2015 Direct patterning of Cu microstructures using femtosecond laser-induced CuO nanoparticle reduction *Japan. J. Appl. Phys.* **54** 06FP07
- [27] Kang B, Han S, Kim J, Ko S and Yang M 2011 One-step fabrication of copper electrode by laser-induced direct local reduction and agglomeration of copper oxide nanoparticle *J. Phys. Chem. C* **115** 23664–70
- [28] Lee H and Yang M 2015 Effect of solvent and PVP on electrode conductivity in laser-induced reduction process *Appl. Phys. A* **119** 317–23
- [29] Ryu J, Kim H and Hahn H T 2011 Reactive sintering of copper nanoparticles using intense pulsed light for printed electronics *J. Electron. Mater.* **40** 42–50
- [30] Bai S, Zhang S, Zhou W, Ma D, Ma Y, Joshi P and Hu A 2017 Laser-assisted reduction of highly conductive circuits based on copper nitrate for flexible printed sensors *Nano-Micro Lett.* **9** 42
- [31] Bhaviripudi S, Jia X, Dresselhaus M S and Kong J 2010 Role of kinetic factors in chemical vapor deposition synthesis of uniform large area graphene using copper catalyst *Nano Lett.* **10** 4128–33
- [32] Lee Y and Choa Y 2012 Adhesion enhancement of ink-jet printed conductive copper patterns on a flexible substrate *J. Mater. Chem.* **22** 12517–22
- [33] Yin Z, Lee C, Cho S, Yoo J, Piao Y and Kim Y S 2014 Facile synthesis of oxidation-resistant copper nanowires toward solution-processable, flexible, foldable, and free-standing electrodes *Small* **10** 5047–52
- [34] Luchan L, Lei L, Peng P, Guisheng Z, Walt W D and Zhou Y N 2016 *In situ* nanojoining of Y- and T-shaped silver nanowires structures using femtosecond laser radiation *Nanotechnology* **27** 125201
- [35] Cong H, Qiu J and Yu S 2015 Thermoresponsive poly(N-isopropylacrylamide)/graphene/Au nanocomposite hydrogel for water treatment by a laser-assisted approach *Small* **11** 1165–70
- [36] Kumar M P, Kesavan T, Kalita G, Ragupathy P, Narayanan T N and Pattanayak D K 2014 On the large capacitance of nitrogen doped graphene derived by a facile route *RSC Adv.* **4** 38689–97
- [37] Ferrari A C and Robertson J 2004 Raman spectroscopy in carbons: from nanotubes to diamond *Philos. Trans. R. Soc. London, Ser. A* **362**
- [38] Peng J, Gao W, Gupta B K, Liu Z, Romeroaburto R, Ge L, Song L, Alemany L B, Zhan X and Gao G 2012 Graphene quantum dots derived from carbon fibers *Nano Lett.* **12** 844–9
- [39] Worsley M A, Pham T, Yan A, Shin S J, Lee J R I, Baggehausen M, Mickelson W and Zettl A 2014 Synthesis and characterization of highly crystalline graphene aerogels *ACS Nano* **8** 11013–22
- [40] Ananthanarayanan A, Wang X, Routh P, Sana B, Lim S, Kim D, Lim K H, Li J and Chen P 2014 Facile synthesis of graphene quantum dots from 3D graphene and their application for Fe₃₊ sensing *Adv. Funct. Mater.* **24** 3021–6
- [41] Gu J, Hu M, Guo Q, Ding Z, Sun X and Yang J 2014 High-yield synthesis of graphene quantum dots with strong green photoluminescence *RSC Adv.* **4** 50141–4
- [42] Peng P, Hu A, Huang H, Gerlich A P, Zhao B and Zhou Y N 2012 Room-temperature pressureless bonding with silver nanowire paste: towards organic electronic and heat-sensitive functional devices packaging *J. Mater. Chem.* **22** 12997–3001
- [43] Peng Z, Lin J, Ye R, Samuel E L G and Tour J M 2015 Flexible and stackable laser-induced graphene supercapacitors *ACS Appl. Mater. Interfaces* **7** 3414–9
- [44] Garnett E C, Cai W, Cha J J, Mahmood F, Connor S T, Greyson Christoforo M, Cui Y, McGehee M D and Brongersma M L 2012 Self-limited plasmonic welding of silver nanowire junctions *Nat. Mater.* **11** 241
- [45] Yang H, Lu J G, Ghosh P, Chen Z, Wang W, Ye H, Yu Q, Qiu M and Li Q 2018 Plasmonic-enhanced targeted nanohealing of metallic nanostructures *Appl. Phys. Lett.* **112** 071108
- [46] Peng P, Hu A and Zhou Y 2012 Laser sintering of silver nanoparticle thin films: microstructure and optical properties *Appl. Phys. A* **108** 685–91
- [47] Pierson H O 1994 *Handbook of Carbon, Graphite, Diamond and Fullerenes. Properties, Processing and Applications* (Park Ridge, NJ: Noyes Publications)
- [48] Stankovich S, Dikin D A, Dommett G H B, Kohlhaas K M, Zimney E, Stach E A, Piner R D, Nguyen S T and Ruoff R S 2006 Graphene-based composite materials *Nature* **442** 282–6
- [49] Fuentescabrera M, Rhodes B H, Fowlkes J D, Lopezbenzanilla A, Terrones H, Simpson M L and Rack P D 2011 Molecular dynamics study of the dewetting of copper on graphite and graphene: implications for nanoscale self-assembly *Phys. Rev. E* **83** 041603
- [50] Franchy R 2000 Growth of thin, crystalline oxide, nitride and oxynitride films on metal and metal alloy surfaces *Surf. Sci. Rep.* **38** 195–294
- [51] Kim I, Kim Y, Woo K, Ryu E, Yon K, Cao G and Moon J 2013 Synthesis of oxidation-resistant core-shell copper nanoparticles *RSC Adv.* **3** 15169–77
- [52] Zhai H, Wang R, Wang X, Cheng Y X, Shi L and Sun J 2016 Transparent heaters based on highly stable Cu nanowire films *Nano Res.* **9** 3924–36
- [53] Chen S, Brown L, Levendorf M, Cai W, Ju S, Edgeworth J, Li X, Magnuson C W, Velamakanni A and Piner R D 2011 Oxidation resistance of graphene-coated Cu and Cu/Ni alloy *ACS Nano* **5** 1321–7